Ultrafast Dynamics within the 1S Exciton Band of Colloidal PbSe Quantum Dots Using Multiresonant Coherent Multidimensional Spectroscopy

Daniel D. Kohler, Stephen B. Block, Schuyler Kain, Andrei V. Pakoulev, and John C. Wright

Department of Chemistry

University of Wisconsin-Madison

1101 University Avenue

Madison, WI 53706

Supporting Information

TEM Characterization

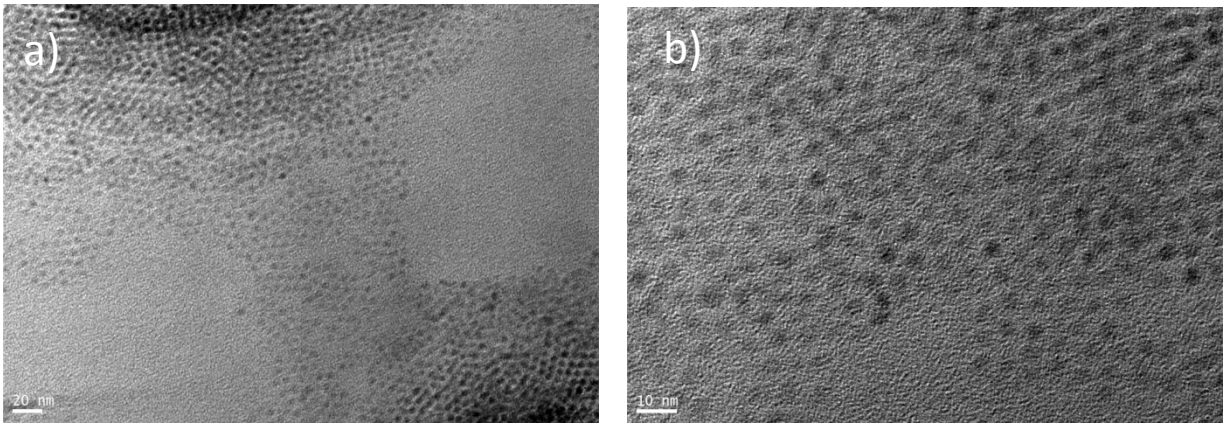

Figure S1. Representative TEM images of PbSe quantum dots. Sample C from the paper is shown.

Non-resonant contributions

The FWM contributions involving states that are far from resonant excitation can lead to interference effects when all three pulses are temporally overlapped. We model such contributions by treating them as a single resonance with large detuning. Thus, the purely driven contribution to the FWM polarization, ρ_{NR}, is given by

$$\rho_{NR}(t) = c_{NR} E_1 E_2 E_{2'} e^{i\theta_{NR}},$$

where $c_{NR}$is the amplitude of the polarization and θ_{NR} is a parameter that accounts for the finite detuning of the states. Through fitting, it was found that $\theta_{NR} \approx 0$ was best for this study, suggesting this contribution to the signal follows the electric fields without any phase lag, which supports the initial assumption of large detuning. Amplitude was found to be 3x-1.5x weaker than the maximum signal of due to quantum dots. The exact ratio depended on concentration and size-dependent dipole strength of quantum dots.

Raman Contributions

In addition to non-resonant output discussed above and fully-resonant pathways discussed in the paper, a family of singly-resonant Raman processes can also contribute to our measured signal. Such output was identified and characterized in a similar sample and matrix using picosecond lasers.[1] Here we adapt the methodology of these Raman processes to apply to our experiments. While the aforementioned studies found signatures of solvent Raman modes in their spectra, we find that the spectra presented here should have minimal contributions from

such features. Conversely, we find that our delay-delay scans have contributions from such processes.

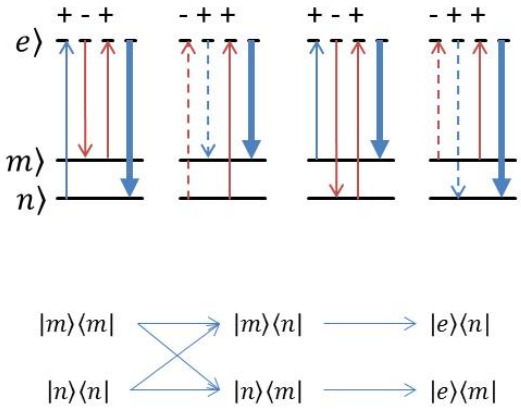

Figure S2. Stimulated Raman pathways detectible in CMDS experiments. The top of the figure shows the WMEL diagrams for such processes involving the ground state manifold of vibrational states (*m* and *n*), and a virtual electronic state (*e*). Due to their large bandwidths, ω_1 and $\omega_{2'}$ can perform either of the transitions marked with a '+' sign. The bottom row shows the Liouville pathways neglecting the initial transition to a virtual state.

For any two vibrational modes in the ground state, there are four stimulated Raman pathways that are phase-matched in the direction of measurement: two Stokes and two anti-Stokes (Figure S2). Contrary to conventional Raman experiments, Stokes and anti-Stokes pathways are not indicative of whether the resonance will occur at positive or negative difference frequencies. In all four pathways, two beams of opposite phase interact first to produce a vibrational coherence between modes *m* and *n*. Neglecting pulse bandwidth, resonant excitation of *mn* and *nm* coherences requires that excitation fields E_1 and E_2 interact before $E_{2'}$ (i.e. pulse time-orderings I or III). Scanning $\tau_{2',1}$ within these pathways will reveal the dynamics of the *mn* and *nm* coherences.

Examination of the Raman Liouville pathways suggests that the spectra presented in this paper are contaminated minimally by Raman pathways, and of the Raman signal that does contribute, it is insensitive to our scanning parameters. The formation of the vibrational coherence can be fully resonant only if E_2 and E_1 form the first two interactions, but, because laser bandwidth is on the order of the vibrational frequencies considered, E_2 and $E_{2'}$ can create this coherence as well. If E_2 and $E_{2'}$ form such a coherence, however, a resonance will not be observed in the frequency domain. Since our frequency-domain experiments focus on time-ordered pathways where E_2 and $E_{2'}$ come before E_1, we do not consider such effects in our spectra.

Phonon Contributions

When scanning over our delay space, however, we can observe the dynamics of the vibrational coherences. Moreover, our bandwidth impulsively excites several vibrational coherences that can beat at their difference frequencies through the coherence evolution time (i.e. positive $\tau_{2',1}$). Figure S3 shows the signal of neat CCl_4 as a function of $\tau_{2',1}$ with τ_{21} = 0 fs, and $\bar{\nu}_1 - \bar{\nu}_2 = 400\ \mathrm{cm}^{-1}$. The frequency components of the exponential-subtracted signal match difference frequencies of well-known Raman modes. The peak at ($\tau_{2',1}$, τ_{21}) = (120, 0) fs and a loss of intensity at (75, 50) fs in figure 4b of the paper is consistent with the beating between the 217 cm^{-1} and the 460 cm^{-1} modes of CCl_4 (135 fs period).

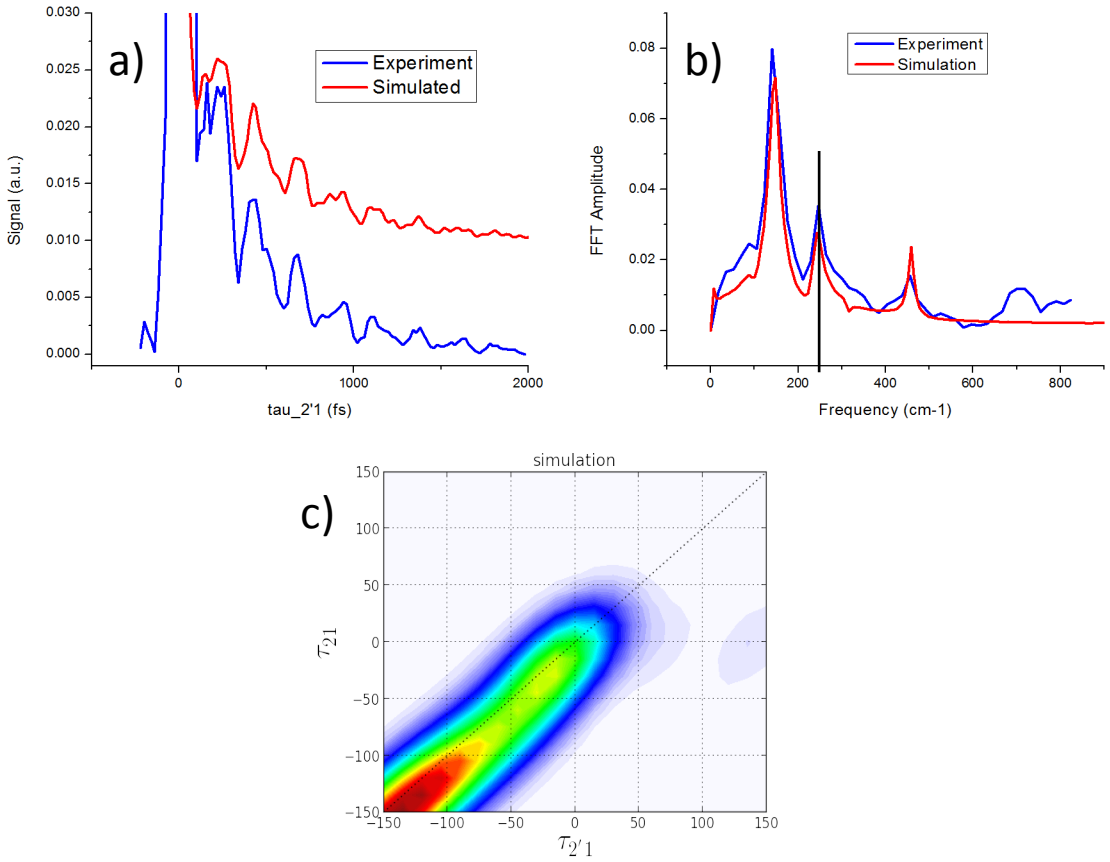

Figure S3: Modeling CCl_4 response and implementation in Quantum dot simulations. (A) Experimental (blue) and simulated (red) response of neat CCl_4. Traces are obtained by scanning scanning c_{2ca} at n_{21} = 0 fs with $\bar{\nu}_1 - \bar{\nu}_2 = 400$ cm^{-1}. Traces were offset vertically for clarity. (B) Fourier transform of the exponential-subtracted traces from A. The interference pattern of the delay transients shows peaks that match the difference frequencies of well-known Raman modes. The black vertical line highlights the beating frequency caused by 460 cm^{-1} and 217 cm^{-1} modes. (C) Simulated quantum dot dynamics with solvent response included. The solvent beating patterns on top of quantum dot signal can produce a signal spike near (τ_{2mo} , τ_{21}) = (135 fs, 0 fs).

Spectral and Temporal Cross-Sections Through the Wigner Plots in Figure 7.

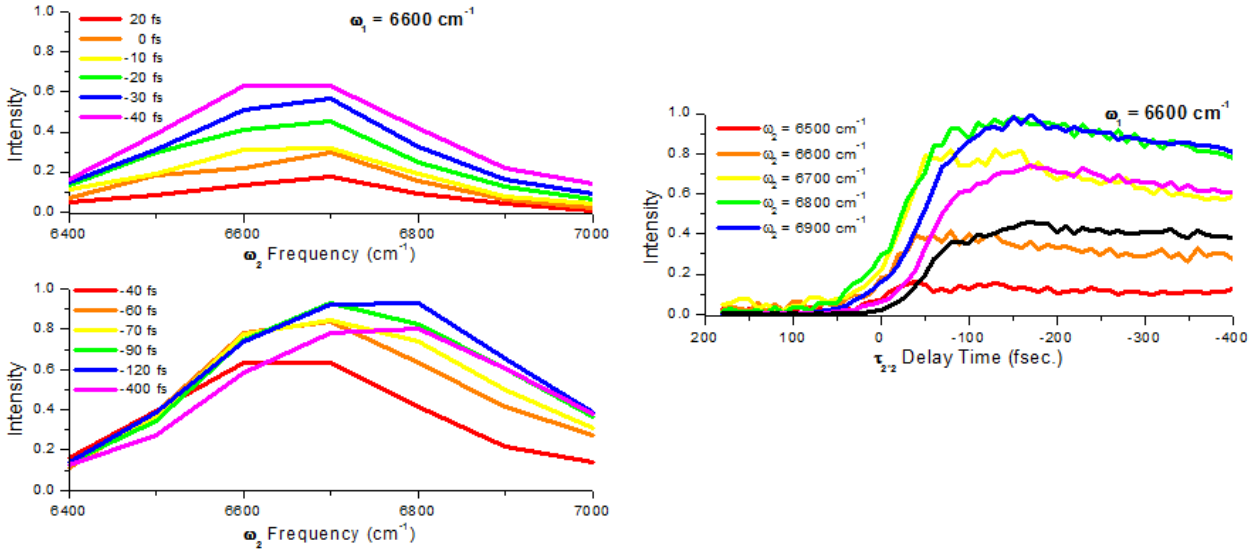

Figure S4- Spectral cross-sections of the data displayed in the Wigner plots shown in Fig. 7 when $\omega_1 = 6600\ cm^{-1}$.

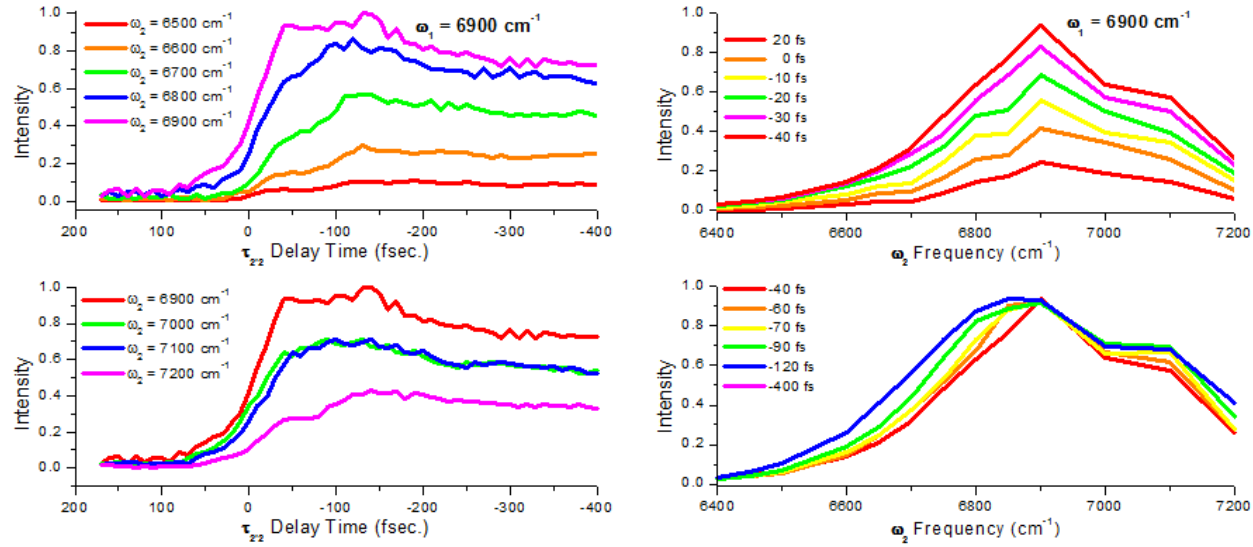

Figure S5- Spectral cross-sections of the data displayed in the Wigner plots shown in Fig. 7 when $\omega_1 = 6900\ cm^{-1}$.

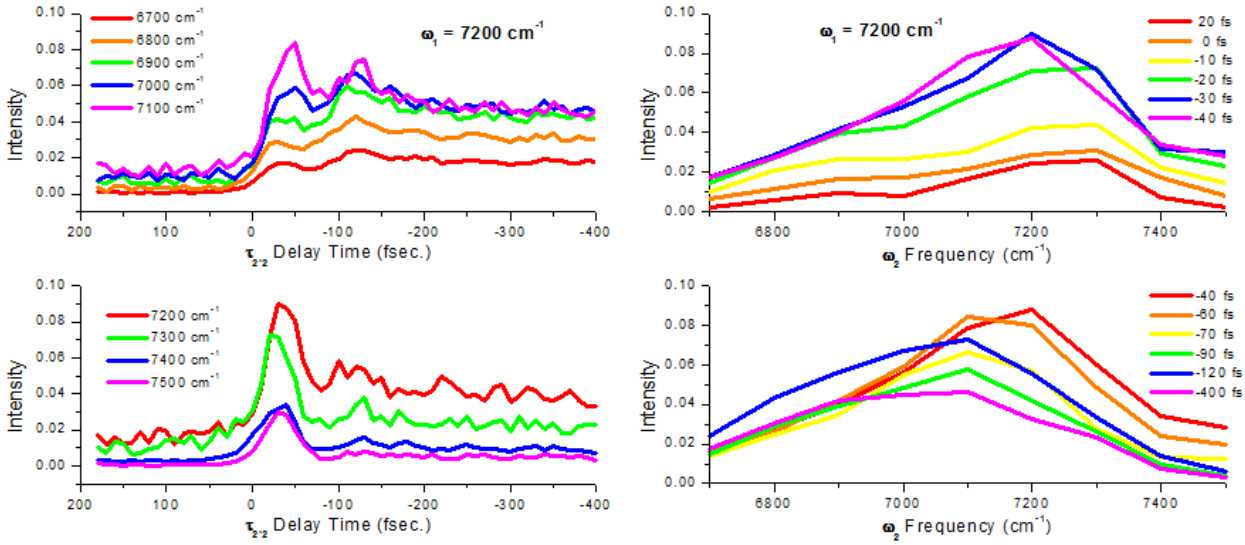

Figure S6- Spectral cross-sections of the data displayed in the Wigner plots shown in Fig. 7 when $\omega_1 = 7200\ cm^{-1}$.

References

(1) Yurs, L. A.; Block, S. B.; Pakoulev, A. V.; Selinsky, R. S.; Jin, S.; Wright, J. *Journal of Physical Chemistry C* **2012**, *116*, 5546-5553.